

# Geometric Resilience of Quantum LiDAR in Turbulent Media: A Wasserstein Distance Approach

Arnaud Coatanhay and Angélique Drémeau  
*Lab-STICC, UMR CNRS 6285, ENSTA, Institut Polytechnique de Paris,  
2 rue François Verny, 29806 Brest Cedex 9, France*

(Dated: March 2, 2026)

Quantum-enhanced LiDAR, exploiting squeezed states of light, promises significant sensitivity gains over classical protocols. However, in realistic scenarios characterized by high optical losses and atmospheric turbulence, standard figures of merit, such as quantum fidelity or the quantum Chernoff bound, saturate rapidly, failing to provide a usable gradient for system optimization. In this work, we propose the Quantum Wasserstein Distance of order 2 ( $W_2$ ) as a robust geometric metric for lossy quantum sensing. Unlike overlap-based measures,  $W_2$  quantifies the transport cost in phase space and maintains a linear response to channel transmissivity, even in regimes where the quantum state is virtually indistinguishable from thermal noise. We derive an analytical threshold for the quantum advantage, demonstrating that squeezing is only beneficial when the transmissivity exceeds a critical value determined by the environmental noise-to-signal ratio. Furthermore, using Monte-Carlo simulations of a fading channel, we show that  $W_2$  acts as a high-fidelity estimator of instantaneous link quality, exhibiting a wide dynamic range immune to the numerical instabilities of fidelity-based metrics. This geometric framework bridges the gap between quantum optimal transport and practical receiver design, paving the way for adaptive sensing in scattering media.

## I. INTRODUCTION

The convergence of quantum information theory and optical engineering has led to a new class of active sensing protocols capable of surpassing classical precision limits [1, 2].

Ranging from seminal quantum illumination protocols for noisy environments [3–7] to the development of microwave quantum radar [8], these advancements herald a paradigm shift in remote sensing.

Within this broad landscape, quantum LiDAR employing squeezed states of light represents a particularly pragmatic approach. Unlike entanglement-based protocols that require storing an idler mode, squeezed sources focus on reducing noise variance in a specific quadrature to achieve sub-shot-noise sensitivity [9, 10]. This strategy has been successfully deployed in gravitational wave observatories [11] and high-efficiency table-top experiments [12].

However, the theoretical advantage of such schemes is often severely challenged in realistic operating environments characterized by strong attenuation and decoherence. In scattering media such as turbid water or fog, the propagation of quantum light is governed by open system dynamics that degrade quantum features. As recently detailed by Kopylov et al. [13], the interaction with a Markovian environment does not merely attenuate the signal; it fundamentally alters the modal structure of the field, rendering standard single-mode descriptions insufficient.

Furthermore, atmospheric turbulence induces stochastic fluctuations in transmissivity (fading), leading to a non-Gaussian mixture of states that complicates the detection process [14, 15]. In this regime of high loss and low SNR, the standard figures of merit for state distinguishability — such as the quantum fidelity or the quan-

tum Chernoff bound — become ill-suited for engineering optimization [16, 17]. Since quantum fidelity measures the overlap between density matrices, it decays exponentially with phase-space displacement [17, 18]. Consequently, for a target located at a significant distance, the fidelity tends rapidly to zero, creating a “blind spot” where the metric saturates and fails to provide a usable gradient for system feedback, even though physical distinguishability (energy difference) remains.

In this paper, we propose to shift the paradigm from overlap-based metrics to transport-based metrics. We introduce the quantum Wasserstein distance of order 2 ( $W_2$ ) as a robust figure of merit for lossy quantum sensing. Originating from the theory of optimal transport [19, 20],  $W_2$  quantifies the minimal “cost” to transform the noise state into the signal state, offering a geometric perspective recently extended to the quantum domain [21]. We derive the analytical expression of  $W_2$  for Gaussian squeezed states propagating in a lossy channel using the Gelbrich formula [22]. We demonstrate that, unlike quantum fidelity, the quantum Wasserstein distance exhibits a linear resilience to losses and fading. Crucially, we show that maximizing  $W_2$  is physically equivalent to optimizing the SNR of a balanced homodyne detector aligned with the “maximally squeezed modes” identified in multimode theories [13, 23]. This approach provides a unified framework for assessing the performance of quantum LiDARs, suggesting new pathways for adaptive sensing in turbulent media where overlap-based metrics diverge [14, 24].

The paper is organized as follows. Section II establishes the physical framework for squeezed probe propagation in dissipative environments, setting the stage for Section III, which bridges quantum geometry and detection theory. We then benchmark the Wasserstein distance against fundamental limits, such as the Quantum

Chernoff Bound, in Section IV. Building on these results, Section V addresses the engineering challenge of optimal resource allocation, before Section VI extends the analysis to realistic fading channels.

## II. PHYSICAL MODEL AND QUANTUM DYNAMICS

In this section, we define the theoretical framework for the generation of the squeezed probe and its subsequent evolution through a dissipative environment, establishing the foundation for our geometric analysis.

### II.1. Squeezed State Preparation

The quantum probe is generated by a degenerate optical parametric oscillator (OPO) operating below threshold. In a simplified spatial propagation model, the evolution of the field operator within the nonlinear crystal is governed by the spatial Heisenberg equation:

$$\frac{d\hat{a}(z)}{dz} = ik\hat{a}(z) + i\Gamma J(z)\hat{a}^\dagger(z), \quad (1)$$

where  $\hat{a}^\dagger(z)$  is the Hermitian conjugate of  $\hat{a}(z)$ ,  $z$  denotes the position along the optical axis,  $k$  is the propagation constant,  $\Gamma$  the nonlinear coupling constant and  $J(z)$  represents the pump-induced coupling profile. In the lossless limit, the resulting output state is a squeezed vacuum, characterized in the quadrature basis  $(\hat{q}, \hat{p})$  by a covariance matrix  $\boldsymbol{\sigma}_{\text{in}} = \text{diag}(e^{-2r}, e^{2r})$ , where  $r$  is the squeezing parameter.

To construct a LiDAR-compatible probe, a coherent displacement  $\alpha$  is applied to the squeezed vacuum, typically via a high-transmissivity beamsplitter and a local oscillator. The resulting output is a displaced squeezed state, characterized by its first-moment vector:

$$\boldsymbol{\mu}_{\text{in}} = \sqrt{2} \begin{pmatrix} \text{Re}(\alpha) \\ \text{Im}(\alpha) \end{pmatrix}. \quad (2)$$

This state serves as our benchmark for quantum-enhanced sensing, combining the directional energy of a laser with the reduced noise floor of squeezing.

### II.2. Propagation in a Lossy Markovian Channel

The interaction between the signal and the scattering environment (e.g., atmosphere or turbid water) is modeled as a bosonic loss channel. As highlighted in recent multimode studies [13], internal losses can be rigorously described by a spatial Langevin equation [25]:

$$\frac{d\hat{a}(z)}{dz} = i\kappa\hat{a}(z) + i\Gamma J(z)\hat{a}^\dagger(z) + \sqrt{\alpha_{\text{loss}}}\hat{f}(z), \quad (3)$$

where  $\kappa \triangleq k + i\alpha_{\text{loss}}/2$  incorporates the extinction coefficient  $\alpha_{\text{loss}}$  and  $\hat{f}(z)$  is the Langevin noise operator associated with the environmental thermal bath.

While the physical attenuation is a continuous process governed by the master equation, the evolution of a Gaussian mode through a memoryless linear loss channel is rigorously mathematically equivalent to a discrete beam splitter interaction [26, 27]. By integrating the Heisenberg-Langevin equation (3) over the propagation distance  $L$ , the continuous decay maps exactly to the input-output relation:

$$\hat{a}_{\text{out}} = \sqrt{\eta}\hat{a}_{\text{in}} + \sqrt{1-\eta}\hat{a}_{\text{env}}, \quad (4)$$

where  $\hat{a}_{\text{in}} \triangleq \hat{a}(0)$  and  $\hat{a}_{\text{out}} \triangleq \hat{a}(L)$  denote the boundary operators. Here,  $\eta \triangleq e^{-\gamma L}$  is the channel transmissivity determined by the linear attenuation coefficient  $\gamma$  and  $\hat{a}_{\text{env}}$  represents the bosonic operator of the environment (thermal bath). This ‘‘fictitious beam splitter’’ model is the standard representation for quantum communication channels [10], as it preserves the canonical commutation relations  $[\hat{a}_{\text{out}}, \hat{a}_{\text{out}}^\dagger] = 1$ .

Since this interaction is linear, it maps Gaussian input states to Gaussian output states. Consequently, the infinite-dimensional evolution of the density matrix is fully captured by the symplectic transformation of its first and second statistical moments. For a round-trip propagation characterized by an effective transmissivity  $\eta$ , the moments evolve according to the following relations:

$$\boldsymbol{\mu}_{\text{out}} = \sqrt{\eta}\boldsymbol{\mu}_{\text{in}}, \quad (5)$$

$$\boldsymbol{\sigma}_{\text{out}} = \eta\boldsymbol{\sigma}_{\text{in}} + (1-\eta)(2n_{\text{th}} + 1)\mathbb{I}, \quad (6)$$

where  $n_{\text{th}}$  represents the mean photon number of the background thermal noise and  $\mathbb{I}$  denotes the identity matrix. This model captures the dual degradation mechanism: the deterministic attenuation of the signal amplitude and the progressive decoherence (anti-squeezing) as the state asymptotically approaches the thermal equilibrium of the environment.

## III. GEOMETRIC METRIC AND DETECTION PERFORMANCE

To quantify the performance of the LiDAR system, we must bridge the gap between the abstract geometry of quantum states and the operational figures of merit used in detection theory. We consider the binary hypothesis testing problem where the receiver must distinguish between the ‘‘target present’’ hypothesis ( $H_1$ , state  $\rho_{\text{out}}$ ) and the ‘‘noise only’’ hypothesis ( $H_0$ , state  $\rho_{\text{env}}$ ).

### III.1. Operational Figure of Merit: Homodyne SNR

We assume the receiver employs balanced homodyne detection, which projects the field onto a quadrature

defined by the Local Oscillator (LO) phase  $\theta$ . In the quadrature basis  $(\hat{q}, \hat{p})$ , the measurement operator is then  $\hat{x}_\theta = \hat{q} \cos \theta + \hat{p} \sin \theta$ .

The distinguishability between the null hypothesis  $H_0$  (target absent) and the alternative hypothesis  $H_1$  (target present) is governed by the Signal-to-Noise Ratio (SNR) of the resulting photocurrent. For Gaussian states, the squared SNR associated with a measurement angle  $\theta$  is given by the deflection coefficient:

$$\text{SNR}^2(\theta) = \frac{|\langle \hat{x}_\theta \rangle_{H_1} - \langle \hat{x}_\theta \rangle_{H_0}|^2}{V_\theta}, \quad (7)$$

where the numerator represents the projected displacement energy –  $\langle \hat{x}_\theta \rangle_{H_1}$  (resp.  $\langle \hat{x}_\theta \rangle_{H_0}$ ) stands for the expectation of measurement  $\hat{x}_\theta$  according to the  $H_1$  (resp.  $H_0$ ) hypothesis –, and the denominator  $V_\theta$  is the noise variance projected along the measurement axis, namely

$$V_\theta \triangleq \mathbf{u}_\theta^T \boldsymbol{\sigma}_{\text{out}} \mathbf{u}_\theta, \quad (8)$$

with  $\mathbf{u}_\theta = (\cos \theta, \sin \theta)^T$ .

In a lossy environment, the state  $\rho_{\text{out}}$  is mixed and rotated. As discussed in [13], standard basis decompositions (such as Mercer-Wolf or Williamson-Euler) do not necessarily yield modes that maximize squeezing utility [13, 23]. Therefore, the optimal detection strategy requires an adaptive search for the ‘‘Maximally Squeezed’’ quadrature. Mathematically, this corresponds to finding the optimal angle  $\theta_{\text{opt}}$  that minimizes the variance  $V_\theta$  (thus maximizing the SNR), effectively aligning the LO with the principal axis of the noise ellipse.

### III.2. The Quantum Wasserstein Distance ( $W_2$ )

In parallel, we consider the quantum Wasserstein distance of order 2 ( $W_2$ ) as a geometric measure of distinguishability. Central to the Monge-Kantorovich optimal transport problem [20] and adapted to quantum systems [19, 21],  $W_2$  quantifies the minimal cost to transform the reference noise state  $\rho_0$  into the signal state  $\rho_1$ .

For two Gaussian states respectively characterized by their first moments  $\boldsymbol{\mu}_0, \boldsymbol{\mu}_1$  and covariance matrices  $\boldsymbol{\sigma}_0, \boldsymbol{\sigma}_1$ , the squared distance is given by the Gelbrich formula [22, 28]:

$$W_2^2(\rho_0, \rho_1) = \underbrace{|\boldsymbol{\mu}_1 - \boldsymbol{\mu}_0|^2}_{\text{Displacement Term}} + \underbrace{\mathcal{B}^2(\boldsymbol{\sigma}_1, \boldsymbol{\sigma}_0)}_{\text{Correlation Term}}, \quad (9)$$

where  $\mathcal{B}^2$  is the Bures distance between the covariance matrices:

$$\mathcal{B}^2(\boldsymbol{\sigma}_1, \boldsymbol{\sigma}_0) = \text{Tr} \left( \boldsymbol{\sigma}_1 + \boldsymbol{\sigma}_0 - 2\sqrt{\boldsymbol{\sigma}_0^{1/2} \boldsymbol{\sigma}_1 \boldsymbol{\sigma}_0^{1/2}} \right). \quad (10)$$

Operationally, in the context of optimal transport, the term  $\mathcal{B}^2(\boldsymbol{\sigma}_0, \boldsymbol{\sigma}_1)$  can be interpreted as a *quantum reshaping cost*. It quantifies the fundamental geometric effort required to transform the covariance structure of state  $\rho_0$  into that of state  $\rho_1$ , completely decoupled from their macroscopic displacement in phase space.

### III.3. Analytical Link with Signal Energy

While standard metrics like Fidelity saturate rapidly in lossy regimes due to the exponential decay of state overlap,  $W_2$  maintains a linear gradient. We now show that  $W_2$  provides a direct geometric measure of the received signal energy, distinct from the signal-to-noise ratio.

Consider the case where the reference state is thermal noise ( $\boldsymbol{\sigma}_0 \propto \mathbb{I}$ ) and the signal is a squeezed state ( $\boldsymbol{\sigma}_1$ ). The optimization of Eq. (7) seeks the direction where the noise variance is minimal (denoted as  $V_{\text{min}}$ ). If the displacement  $\delta\boldsymbol{\mu} \triangleq \boldsymbol{\mu}_{\text{out}} - \boldsymbol{\mu}_{\text{in}}$  is aligned with the squeezed quadrature (the optimal configuration), the operational SNR scales as:

$$\text{SNR}_{\text{opt}}^2 \propto \frac{|\delta\boldsymbol{\mu}|^2}{V_{\text{min}}}. \quad (11)$$

Analyzing the Wasserstein expression in Eq. (9), we observe that the metric naturally decouples the transport of the first moments from the reshaping of the second moments [20, 21]. Applying this to our specific LiDAR scenario (with  $\rho_0 = \rho_{\text{env}}$  and  $\rho_1 = \rho_{\text{out}}$ ), the distance writes:

$$W_2^2(\rho_{\text{out}}, \rho_{\text{env}}) = |\delta\boldsymbol{\mu}|^2 + \mathcal{B}^2(\boldsymbol{\sigma}_{\text{out}}, \boldsymbol{\sigma}_{\text{env}}). \quad (12)$$

In a typical LiDAR scenario, the transport cost is dominated by the displacement of the mean field (signal energy), while the covariance reshaping  $\mathcal{B}^2(\boldsymbol{\sigma}_{\text{out}}, \boldsymbol{\sigma}_{\text{env}})$  remains a second-order geometric correction. Consequently, unlike the SNR which scales with the inverse variance, the Wasserstein distance scales linearly with the square of the coherent amplitude  $|\alpha|^2$ :

$$W_2^2 \approx 2\eta|\alpha|^2. \quad (13)$$

This linear proportionality to the signal intensity – rather than the signal-to-noise ratio – is precisely what prevents the metric from saturating in high-loss scenarios, effectively making  $W_2$  a robust estimator of the channel transmissivity  $\eta$ .

This result is fundamental as calculating the Wasserstein distance  $W_2$  quantifies the geometric availability of the signal, effectively proxying the ideal response of a homodyne detector perfectly matched to the ‘‘Maximally Squeezed’’ mode identified in multimode theory [13]. Consequently,  $W_2$  serves as a robust, parameter-free observable for optimizing the spatial mode matching in scattering media.

## IV. BENCHMARKING AGAINST FUNDAMENTAL LIMITS

To validate the relevance of the Wasserstein distance as a detection metric, we compare its behavior against the fundamental limits of quantum hypothesis testing. The ultimate lower bound on the error probability  $P_{\text{err}}$

for distinguishing two states  $\rho_0$  and  $\rho_1$  is given by the Helstrom bound. In the asymptotic limit of large data samples  $M$ , this error scales as  $P_{\text{err}} \sim \exp(-M\xi_{\text{QCB}})$ , where  $\xi_{\text{QCB}}$  is the Quantum Chernoff Bound [16], defined as:

$$\xi_{\text{QCB}} = -\ln \left( \min_{0 \leq s \leq 1} \text{Tr}[\rho_0^s \rho_1^{1-s}] \right). \quad (14)$$

#### IV.1. The Quantum Bhattacharyya Proxy

Calculating  $\xi_{\text{QCB}}$  exactly requires a complex minimization over the power  $s \in [0, 1]$ . A standard, computationally tractable alternative – serving as a worst-case scenario – is the Quantum Bhattacharyya Bound (QBB), obtained by setting  $s = 0.5$ . Because  $\xi_{\text{QBB}} \leq \xi_{\text{QCB}}$ , it serves as a conservative lower bound for the error exponent.

Furthermore, the QBB is intrinsically related to the quantum fidelity  $F(\rho_0, \rho_1) \triangleq \|\sqrt{\rho_0}\sqrt{\rho_1}\|_1^2$  [17, 29]. Specifically, for pure or commuting states, the Bhattacharyya coefficient simplifies exactly to  $F(\rho_0, \rho_1)$ , yielding:

$$\xi_{\text{QBB}} = -\ln \text{Tr}[\sqrt{\rho_0}\sqrt{\rho_1}] = -\frac{1}{2} \ln F(\rho_0, \rho_1). \quad (15)$$

This quantity represents the exponential decay rate of the state overlap. While physically rigorous, fidelity-based metrics suffer from a major drawback in engineering contexts: in lossy or noisy regimes, the overlap between the signal and the thermal background vanishes exponentially [18], leading to numerical saturation [10].

#### IV.2. Metric Resilience in Lossy Regimes

Figure 1 compares the evolution of our geometric metric  $W_2^2$  against the Bhattacharyya bound  $\xi_{\text{QBB}}$  as a function of channel transmissivity  $\eta$ . The simulation parameters are set to a representative scenario with total energy  $N_{\text{tot}} = 5$  photons and a high thermal noise background  $n_{\text{th}} = 2$ , typical of daylight operation.

As observed in Fig. 1, the QBB (red dashed line) exhibits a “digital” behavior: it is high for good transmission but saturates or diverges when  $\eta \rightarrow 0$ . This implies that the signal state  $\rho_{\text{out}}$  becomes effectively orthogonal to the vacuum in the high-dimensional Hilbert space, not because of signal strength, but due to thermal dilution.

In contrast, the squared Wasserstein distance (blue solid line) decays linearly with  $\eta$ . This linearity is a direct consequence of the geometric property of optimal transport:

$$W_2^2(\Phi_\eta(\rho), \Phi_\eta(\sigma)) \approx \eta W_2^2(\rho, \sigma), \quad (16)$$

where  $\Phi_\eta$  denotes the completely positive trace-preserving (CPTP) map associated with the lossy channel of transmissivity  $\eta$ .

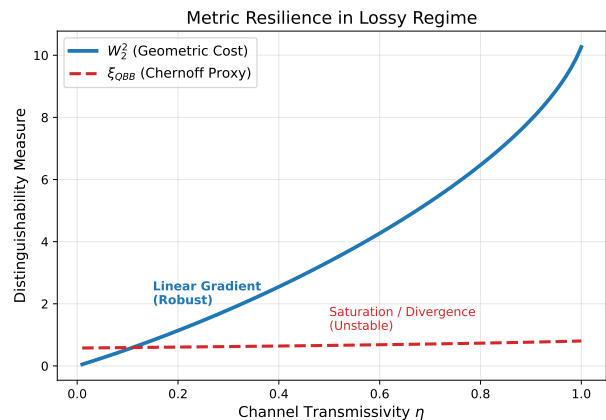


FIG. 1. Benchmarking distinguishability metrics in a high-loss environment ( $N_{\text{tot}} = 5, n_{\text{th}} = 2$ ). The Quantum Bhattacharyya Bound ( $\xi_{\text{QBB}}$ , dashed red) saturates rapidly, indicating a vanishing state overlap that hinders gradient-based optimization. In contrast, the Wasserstein distance ( $W_2^2$ , solid blue) maintains a robust linear behavior, providing a continuous “transport cost” gradient even in regimes where the quantum states are nearly indistinguishable by overlap.

Crucially, this means that  $W_2$  provides a *non-vanishing gradient* for optimization. Even when the probability of error is nearing 0.5 (states overlapping significantly),  $W_2$  quantifies the residual “energy cost” required to distinguish them. This makes it a superior cost function for adaptive feedback loops in scattering media, where fidelity-based metrics typically fail to provide a direction for improvement.

### V. OPTIMAL RESOURCE ALLOCATION AND DISCUSSION

Having established the robustness of the Wasserstein metric, we now address the central engineering problem: given a finite energy budget  $N_{\text{tot}}$ , how should resources be distributed between coherent displacement (signal intensity) and squeezing (noise reduction) to maximize target distinguishability?

We define the squeezing fraction  $\lambda \in [0, 1]$  such that the mean photon numbers allocated to squeezing and displacement are  $N_{\text{sq}} = \lambda N_{\text{tot}}$  and  $N_{\text{disp}} = (1 - \lambda) N_{\text{tot}}$ , respectively.

#### V.1. The Quantum-Classical Phase Transition

Figure 2 maps the detection performance, quantified by  $W_2^2$ , as a joint function of the channel transmissivity  $\eta$  and the squeezing fraction  $\lambda$ . The simulation assumes a low-noise scenario ( $N_{\text{tot}} = 10, n_{\text{th}} = 0.1$ ), representative of a system operating with narrow spectral filtering or in nighttime conditions.

The white dashed line in Fig. 2 traces the optimal strategy, defined as the allocation that maximizes the distinguishability:  $\lambda_{\text{opt}}(\eta) \triangleq \arg \max_{\lambda} W_2^2(\lambda, \eta)$ .

We formally define the ‘‘Classical Regime’’ as the domain where no resources should be allocated to squeezing ( $\lambda_{\text{opt}} \rightarrow 0$ ), meaning a purely coherent state is optimal. Conversely, the ‘‘Quantum Regime’’ designates the domain where injecting squeezed vacuum strictly improves the detection metric ( $\lambda_{\text{opt}} > 0$ ). A clear crossover behavior is observed. In the high-transmissivity regime ( $\eta \rightarrow 1$ ), the optimal strategy allocates significant resources to squeezing, validating the quantum advantage. However, as losses increase, the system undergoes a transition to a ‘‘Classical Regime’’ where  $\lambda_{\text{opt}} \rightarrow 0$ . In this domain, the most efficient strategy is to concentrate all energy into the displacement vector  $\boldsymbol{\mu}$ , as the covariance advantage provided by squeezing is washed out by the vacuum admixture.

## V.2. Analytical Threshold of Quantum Advantage

To provide a rigorous justification for the phase transition observed in Fig. 2, we perform a perturbative analysis of the Wasserstein distance in the limit of small squeezing allocation ( $\lambda \ll 1$ ). Let the total energy be fixed at  $N_{\text{tot}}$ . We analyze the variation of the detection metric  $W_2^2$  when a small fraction of energy is transferred from the displacement to the squeezing.

In that particular context, the exact energy allocations are defined as  $N_{\text{disp}} = (1 - \lambda)N_{\text{tot}}$  and  $N_{\text{sq}} = \lambda N_{\text{tot}}$ . Re-

calling that the mean photon number of a squeezed vacuum mode is strictly given by  $N_{\text{sq}} = \sinh^2(r)$ , the state parameters in the perturbative limit ( $\lambda \ll 1$ ) simplify to:

$$N_{\text{disp}} \approx N_{\text{tot}}, \quad (17)$$

$$r \approx \sqrt{\lambda N_{\text{tot}}}. \quad (18)$$

As shown in Eq. (9), the squared Wasserstein distance decomposes into a classical displacement term and a quantum covariance term. For clarity, we denote these terms as  $\mathcal{D}^2$  and  $\mathcal{K}^2$ , respectively. This decomposition allows us to treat the optimization as a competition between two distinct gradients.

On the one hand, the displacement term decays linearly with the squeezing fraction  $\lambda$ :

$$\frac{\partial \mathcal{D}^2}{\partial \lambda} = -2\eta N_{\text{tot}}. \quad (19)$$

This represents the ‘‘classical cost’’ of diverting power from the carrier.

On the other hand, the covariance term measures the geometric transport from the thermal reference  $\sigma_{\text{th}} = (2n_{\text{th}} + 1)\mathbb{I}$  to the squeezed state. Using the Taylor expansion of the Bures metric for an infinitesimal squeezing parameter, the geometric transport from the thermal reference  $\sigma_{\text{th}} = (2n_{\text{th}} + 1)\mathbb{I}$  can be approximated. A second-order expansion with respect to the squeezing fraction  $\lambda$  yields the marginal quantum gain:

$$\left. \frac{\partial \mathcal{K}^2}{\partial \lambda} \right|_{\lambda=0} \approx \frac{2\eta^2 N_{\text{tot}}}{2n_{\text{th}} + 1} \left( 1 + \frac{N_{\text{tot}}}{2n_{\text{th}} + 1} \right). \quad (20)$$

The ‘‘Quantum Regime’’ is accessible if and only if this marginal quantum gain strictly compensates the classical cost of diverting power from the carrier. We formalize this competition as:

$$\left. \frac{\partial W_2^2}{\partial \lambda} \right|_{\lambda=0} = \underbrace{-2\eta N_{\text{tot}}}_{\text{Classical Cost}} + \underbrace{\frac{2\eta^2 N_{\text{tot}}}{2n_{\text{th}} + 1} \left( 1 + \frac{N_{\text{tot}}}{2n_{\text{th}} + 1} \right)}_{\text{Marginal Quantum Gain}} > 0. \quad (21)$$

By factoring out  $2\eta N_{\text{tot}}$  (assuming non-zero transmissivity and energy), we can solve this inequality for the channel transmissivity  $\eta$ . This directly leads to the critical threshold  $\eta_c$ . For the quantum advantage to exist, the channel transmissivity must satisfy:

$$\eta > \eta_c \approx \frac{2n_{\text{th}} + 1}{1 + \frac{N_{\text{tot}}}{2n_{\text{th}} + 1}}. \quad (22)$$

Equation (22) analytically confirms the simulation results by revealing a direct competition between noise and power. On the one hand, as the environmental noise  $n_{\text{th}}$  increases, the numerator grows, pushing  $\eta_c \rightarrow 1$  and effectively closing the quantum window. On the other hand, an increase in the probe energy  $N_{\text{tot}}$  expands the denominator, driving  $\eta_c \rightarrow 0$ . Consequently, high-power probes can sustain a quantum advantage even in high-loss regimes.

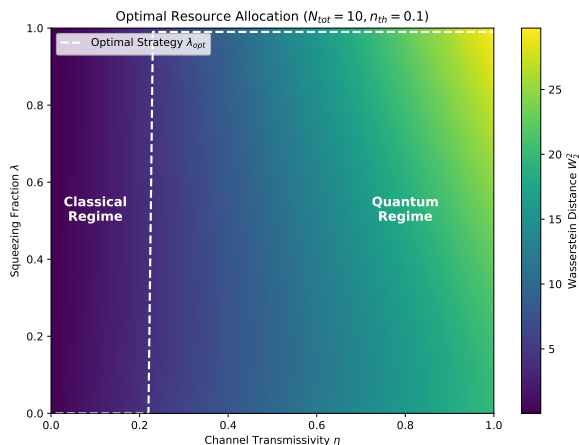


FIG. 2. Map of the optimal resource allocation strategy for a fixed energy budget ( $N_{\text{tot}} = 10$ ) in a low-noise environment ( $n_{\text{th}} = 0.1$ ). The color gradient represents the detection score ( $W_2^2$ ). The white dashed line tracks the optimal squeezing fraction  $\lambda_{\text{opt}}$ . We observe a phase transition: for  $\eta > 0.25$ , the system enters a ‘‘Quantum Regime’’ where maximizing squeezing ( $\lambda \rightarrow 0.95$ ) is beneficial. Below this threshold, the optimal strategy collapses to the ‘‘Classical Regime’’ ( $\lambda \rightarrow 0$ ), as the fragility of squeezed states to loss outweighs their geometric advantage.

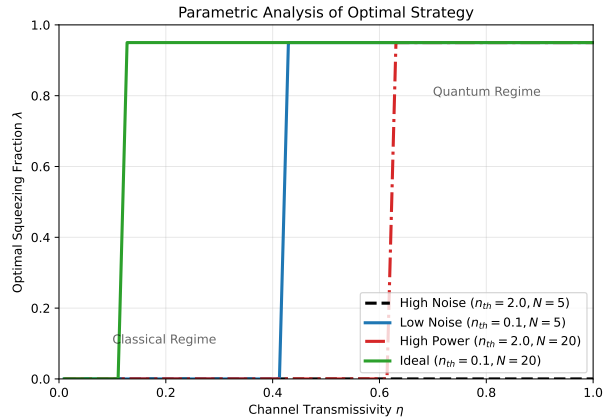


FIG. 3. Parametric analysis of the optimal squeezing fraction versus channel transmissivity. The transition from classical ( $\lambda = 0$ ) to quantum ( $\lambda > 0$ ) strategies is dictated by the thermal noise floor. In high-noise environments ( $n_{\text{th}} = 2.0$ , black dashed line), the quantum advantage is suppressed until  $\eta > 0.5$ . Reducing the noise ( $n_{\text{th}} = 0.1$ , blue solid line) or increasing the signal power ( $N_{\text{tot}} = 20$ , red line) significantly expands the operational range of the quantum regime.

### V.3. Environmental Constraints and Robustness

The position of this quantum-classical boundary is critically dependent on environmental parameters. Figure 3 presents a parametric study of the optimal strategy  $\lambda_{\text{opt}}(\eta)$  for varying noise temperatures  $n_{\text{th}}$  and energy budgets  $N_{\text{tot}}$ .

Analyzing these curves reveals that thermal noise acts as the primary suppressor of quantum advantage. Comparing the high-noise ( $n_{\text{th}} = 2.0$ , black dashed) and low-noise ( $n_{\text{th}} = 0.1$ , blue solid) regimes shows that in a hot environment, injected thermal photons rapidly fill the squeezed uncertainty ellipse, effectively thermalizing the state. The  $W_2$  metric accurately captures this physics, indicating that maintaining squeezing under such conditions is energetically wasteful compared to simply increasing the signal-to-noise ratio via displacement.

To counteract this degradation, power scaling plays a crucial role. As evidenced by increasing the total energy from  $N_{\text{tot}} = 5$  to  $N_{\text{tot}} = 20$  (red line), the transition threshold shifts toward lower transmissivities. This dynamic demonstrates that high-power quantum LiDARs can sustain their advantage deeper into scattering media, provided the initial squeezing is robust enough to survive the attenuation.

### V.4. Impact of Experimental Imperfections

Our model initially assumes ideal detection. However, in a realistic experimental setup, the atmospheric transmission  $\eta_{\text{atm}}$  and the detector efficiency  $\eta_{\text{det}}$  combine to yield an overall transmissivity  $\eta_{\text{tot}} = \eta_{\text{atm}}\eta_{\text{det}}$ . Further-

more, practical homodyne detectors inevitably introduce an additional electronic noise component, denoted by  $v_{\text{el}}$ . Within our Gaussian framework, this electronic noise can be modeled as an excess thermal noise added to the environment term such that

$$\bar{n}_{\text{eff}} = n_{\text{th}} + \frac{v_{\text{el}}}{2(1-\eta)}. \quad (23)$$

Crucially, the derived threshold in Eq. (22) remains valid if one replaces  $\eta$  and  $n_{\text{th}}$  with their respective experimental parameters  $\eta_{\text{tot}}$  et  $\bar{n}_{\text{eff}}$ . This implies that detectors exhibiting electronic noise above the Shot Noise Limit ( $v_{\text{el}} > 1$  SNL) will artificially raise the “thermal barrier,” requiring higher squeezing levels to recover the quantum advantage.

### V.5. Discussion

The results presented in Figs. 2 and 3 offer a framework for optimizing quantum state preparation. Unlike conventional systems that operate with fixed parameters, an optimal receiver should dynamically adjust the squeezing ratio  $\lambda$  based on real-time estimates of the atmospheric extinction  $\eta$  and background noise  $n_{\text{th}}$ . The Wasserstein distance provides the necessary convex cost function to drive this feedback loop, ensuring that the system operates at the true global maximum of distinguishability, seamlessly switching between classical intensity sensing and quantum-enhanced precision as conditions evolve.

## VI. ROBUSTNESS IN FADING CHANNELS

In real-world scenarios such as atmospheric LiDAR or underwater sensing, the assumption of a static transmissivity  $\eta$  breaks down. Turbulence, beam wandering, and scattering inhomogeneities cause the transmissivity to fluctuate stochastically, a phenomenon known as *fading* [14, 15]. The received state is then described by a statistical mixture over the probability distribution  $P(\eta)$  [14, 15]:

$$\rho_{\text{fading}} = \int_0^1 P(\eta)\rho_{\text{out}}(\eta)d\eta. \quad (24)$$

This loss of Gaussianity poses a severe challenge for detection metrics. To evaluate the robustness of our geometric approach, we perform a Monte-Carlo simulation of a turbulent channel.

### VI.1. Turbulence Model and Simulation

We model the fluctuating transmissivity  $\eta$  using a Beta distribution,  $P(\eta) \propto \eta^{\alpha-1}(1-\eta)^{\beta-1}$ , which is widely used

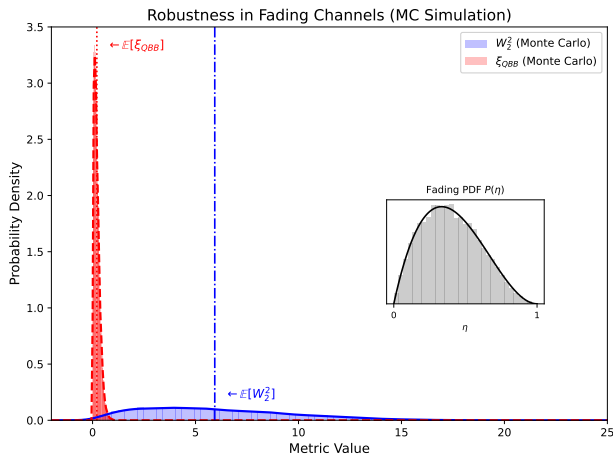


FIG. 4. Statistical distribution of detection metrics in a turbulent fading channel (Monte Carlo simulation,  $10^4$  realizations). The inset shows the probability distribution of the channel transmissivity  $\eta$ . The Wasserstein metric (blue) exhibits a wide dynamic range, mirroring the channel fluctuations. In contrast, the fidelity-based metric (red) is compressed into a narrow spike due to logarithmic saturation. This contrast highlights that  $W_2$  acts as a sensitive estimator of instantaneous link quality, whereas  $\xi_{\text{QBB}}$  flattens the information.

to describe bounded fading processes in free-space optics [14, 30] and is consistent with standard atmospheric turbulence models [31, 32]. To capture a realistic moderate turbulence scenario, we set the shape parameters to  $\alpha = 2$  and  $\beta = 3$ . This specific choice yields a broad, right-skewed distribution with a mean transmissivity of  $\bar{\eta} = 0.4$ , effectively mimicking a channel subjected to significant scintillation without suffering from complete, catastrophic fading. Operating under a fixed resource allocation strategy ( $N_{\text{tot}} = 10$ , with a splitting fraction  $\lambda = 0.5$ ), we generate  $10^4$  independent channel realizations to compute the statistical distributions of both the squared Wasserstein distance  $W_2^2$  and the Quantum Bhattacharyya Bound  $\xi_{\text{QBB}}$ .

## VI.2. Sensitivity and Dynamic Range Analysis

Figure 4 displays the probability density functions (PDFs) of the two metrics, offering a crucial insight into their respective sensitivities. The Wasserstein distribution (blue) exhibits a wide dynamic range that closely mirrors the channel transmissivity, confirming the linear response derived in Eq. (13). In this context, the high variance of  $W_2$  is fundamentally a feature: it acts as a high-fidelity channel estimator, yielding a signal directly proportional to the instantaneous link quality  $\eta(t)$ .

Conversely, the QBB distribution (red) is starkly compressed into a narrow spike near zero, reflecting the severe saturation of fidelity-based metrics in high-loss regimes. As the signal vanishes ( $\eta \rightarrow 0$ ), the received state be-

comes entirely indistinguishable from the thermal background. This causes the fidelity overlap to saturate and the distance metric to flatten, rendering  $\xi_{\text{QBB}}$  effectively blind to the nuances of the fading process.

Consequently, this result has immediate practical implications for post-selection protocols (commonly referred to as “Lucky Imaging”), where the receiver only retains data acquired during moments of high atmospheric transmissivity. While the saturation of fidelity-based metrics tends to mask channel fluctuations—making “good” frames mathematically indistinguishable from “average” ones due to signal compression—the broad dynamic range of the  $W_2$  distribution allows for precise state discrimination. Thus,  $W_2$  acts as a robust observable for the instantaneous link quality, enabling the successful implementation of such filtering based on the true transmissivity  $\eta(t)$ .

## VII. CONCLUSION AND OUTLOOK

In this work, we have addressed the fundamental challenge of optimizing quantum LiDARs in high-loss environments, where standard figures of merit typically fail. By adopting a geometric perspective based on the Quantum Wasserstein distance ( $W_2$ ), we demonstrated that the distinguishability of quantum states can be robustly quantified even when the state overlap vanishes. Unlike the Fidelity or the Quantum Bhattacharyya Bound, which exhibit logarithmic saturation in high-loss regimes, we showed that the  $W_2$  metric maintains a linear gradient with respect to the channel transmissivity. This crucial geometric linearity provides a non-vanishing cost function that is essential for sustaining gradient-based optimization loops.

Building upon this resilient metric, we derived the optimal energy allocation strategy between coherent displacement and squeezing. Crucially, this analysis establishes an analytical threshold for the quantum advantage (Eq. (22)), providing a rigorous design criterion: squeezing is only beneficial when the channel transmissivity  $\eta$  exceeds a critical value determined by the ratio of environmental noise to signal power. Furthermore, by extending our model to turbulent channels via Monte Carlo simulations, we demonstrated that  $W_2$  acts as a high-fidelity estimator of instantaneous link quality. While overlap-based metrics are blind to the nuances of deep fades due to signal compression, the wide dynamic range of  $W_2$  allows for precise “soft-decision” decoding and effective post-selection (Lucky Imaging) in fluctuating media.

Looking forward, this work paves the way for two main research directions. First, the experimental validation of the  $W_2$ -based feedback loop in complex scattering environments stands as a natural next step, particularly to assess the impact of the detector imperfections discussed in Sec. V. Second, our theoretical framework could be extended beyond the Gaussian approximation to eval-

uate non-Gaussian resources, such as Schrödinger cat states [33] or GKP codes [34]. Exploring these states may unveil entirely new geometric advantages within the optimal transport metric landscape.

## ACKNOWLEDGMENTS

The authors gratefully acknowledge the support of the Defense Innovation Agency (AID – Agence de l’Innovation de Défense), French Ministry of the Armed Forces.

- 
- [1] S. L. Braunstein and C. M. Caves, *Physical Review Letters* **72**, 3439 (1994).
- [2] M. G. A. Paris, *International Journal of Quantum Information* **7**, 125 (2009).
- [3] S. Lloyd, *Science* **321**, 1463 (2008).
- [4] S.-H. Tan, B. I. Erkmen, V. Giovannetti, S. Guha, S. Lloyd, L. Maccone, S. Pirandola, and J. H. Shapiro, *Physical Review Letters* **101**, 253601 (2008).
- [5] E. D. Lopaeva, I. Ruo Berchera, I. P. Degiovanni, S. Olivares, G. Brida, and M. Genovese, *Physical Review Letters* **110**, 153603 (2013).
- [6] Z. Zhang, S. Mouradian, F. N. C. Wong, and J. H. Shapiro, *Physical Review Letters* **114**, 110506 (2015).
- [7] S. Borderieux, A. Coatanhay, and A. Khenchaf, *Sensors* **22**, 4821 (2022).
- [8] S. Barzanjeh, S. Guha, C. Weedbrook, D. Vitali, J. H. Shapiro, and S. Pirandola, *Physical Review Letters* **114**, 080503 (2015).
- [9] R. Schnabel, N. Mavalvala, D. E. McClelland, and P. K. Lam, *Nature Communications* **1**, 121 (2010).
- [10] S. Pirandola, B. Bardhan, T. Gehring, C. Weedbrook, and S. Lloyd, *Nature Photonics* **12**, 724 (2018).
- [11] The LIGO Scientific Collaboration, *Nature Physics* **7**, 962 (2011).
- [12] H. Vahlbruch, M. Mehmet, K. Danzmann, and R. Schnabel, *Physical Review Letters* **117**, 110801 (2016).
- [13] D. A. Kopylov, T. Meier, and P. R. Sharapova, *Quantum* **9**, 1621 (2025).
- [14] D. Vasylyev, A. Semenov, and W. Vogel, *Physical Review Letters* **108**, 220501 (2012).
- [15] A. Semenov and W. Vogel, *Physical Review A* **80**, 021802 (2009).
- [16] K. M. Audenaert, J. Calsamiglia, R. Muñoz-Tapia, E. Bagan, L. Masanes, A. Acín, and F. Verstraete, *Physical Review Letters* **98**, 160501 (2007).
- [17] L. Banchi, S. L. Braunstein, and S. Pirandola, *Physical Review Letters* **115**, 260501 (2015).
- [18] C. Weedbrook, S. Pirandola, R. García-Patrón, N. J. Cerf, T. C. Ralph, J. H. Shapiro, and S. Lloyd, *Rev. Mod. Phys.* **84**, 621 (2012).
- [19] K. Zyczkowski and W. Słomczynski, *Journal of Physics A: Mathematical and General* **31**, 9095 (1998).
- [20] C. Villani, *Optimal transport: old and new*, Vol. 338 (Springer, 2009).
- [21] G. De Palma, M. Marvian, D. Trevisan, and S. Lloyd, *IEEE Trans. Inf. Theory* **67**, 6627 (2021).
- [22] M. Gelbrich, *Mathematische Nachrichten* **147**, 185 (1990).
- [23] A. Christ, K. Laiho, A. Eckstein, K. N. Cassemiro, and C. Silberhorn, *New Journal of Physics* **13**, 033027 (2011).
- [24] M. Bohmann, J. Sperling, A. A. Semenov, and W. Vogel, *Phys. Rev. A* **95**, 012324 (2017).
- [25] W. Wasilewski, A. Lvovsky, K. Banaszek, and C. Radzewicz, *Physical Review A* **73**, 063819 (2006).
- [26] U. Leonhardt, *Measuring the quantum state of light* (Cambridge University Press, 1997).
- [27] A. Serafini, *Quantum continuous variables: a primer of theoretical methods* (CRC Press, 2017).
- [28] R. Bhatia, T. Jain, and Y. Lim, *Expositiones Mathematicae* **37**, 165 (2019).
- [29] S. Pirandola and S. Lloyd, *Physical Review A* **78**, 012331 (2008).
- [30] V. C. Usenko, B. Heim, C. Peuntinger, C. Wittmann, C. Marquardt, G. Leuchs, and R. Filip, *New Journal of Physics* **14**, 093048 (2012).
- [31] L. C. Andrews and R. L. Phillips, *Laser beam propagation through random media* (SPIE press, 2005).
- [32] V. I. Tatarski, *Wave propagation in a turbulent medium* (Dover Publications, 2016).
- [33] A. Ourjoumtsev, H. Jeong, R. Tualle-Brouri, and P. Grangier, *Nature* **448**, 784 (2007).
- [34] D. Gottesman, A. Kitaev, and J. Preskill, *Physical Review A* **64**, 012310 (2001).